

Uncovering the physical origin of self-phasing in coupled fiber lasers

Hung-Sheng Chiang* and James R. Leger

Department of Electrical and Computer Engineering, University of Minnesota, Minneapolis, MN,
USA 55455-0170;

ABSTRACT

We studied coherent beam combining in a specific laser cavity architecture in which two Ytterbium-doped fiber amplifiers are passively coupled using a homemade binary phase Dammann grating. Our experimental results show that coherent beam combining is robust against phase perturbation in such a laser cavity architecture when the operating point is sufficiently above the lasing threshold. We observed redistribution of energy within the supermode of this laser cavity in response to an externally applied path length error. The energy redistribution is accompanied by an internal differential phase shift between the coherently coupled gain arms. Self-phasing mitigates or even completely neutralizes the externally applied optical path length error. We identify the physical origin of the observed self-phasing with the resonant (gain related) nonlinearity in the gain elements under our experimental conditions.

Keywords: Coherent beam combining, Ytterbium-doped fiber amplifier, binary phase Dammann grating, self-phasing, resonant nonlinearity

1. INTRODUCTION

Coherent beam combining has been a popular strategy in achieving high-brightness, single-spatial-mode laser outputs. Technically, it can be divided into two categories: an active phasing approach and a passive phasing approach. In the first category, external electronic control loops are employed in order to constantly monitor and correct the phase errors between the combined gain elements. Up to eight Ytterbium-doped fiber amplifiers had been actively phase locked in a tiled-aperture configuration with 78% beam combining efficiency and an output power of 4 kW¹. In the second category, correctly phasing the combined gain elements is accomplished by clever laser cavity design features that favor the in-phase supermode oscillations. Using a phase-contrast technique, Jeux *et al.* were able to passively couple 20 ring fiber lasers at a 78% phase locking level².

Over the past decade, a large volume of theoretical work concerning passive phasing in coherent laser arrays has been published. It was shown that coherent combining efficiency in the presence of resonant (gain related) and Kerr nonlinearities can greatly exceed that predicted by cold-cavity theories³⁻⁵. This was demonstrated very impressively in a recent experiment in which 35 diode lasers were coherently combined by passive phasing mechanism using a Self-Fourier cavity design⁶. Besides the coherent combining efficiency, another important technical aspect regarding a passively phase-locked array is its susceptibility to phase perturbations in an unprotected environment. In an experiment conducted by Guillot *et al.*, a short phase perturbation (5π radians over a duration of 1 ns) was generated in one of the gain branches in a passively phase-locked two-element fiber laser array by cross-phase modulation⁷. They observed that the laser array restored to the original in-phase operation within a time period of just a few cavity round trips after the perturbation, but it took longer time (a few μ s) for their laser to return to its initial output power level.

The important roles that Kerr and resonant nonlinearities play in passive coherent combination of gain elements are gradually being revealed through numerous theoretical and experimental efforts worldwide. Up to the present, however, the experiments that explicitly quantitatively link the passive phasing behaviors to specific nonlinearities present in the combined elements are still few in number. In this review paper, we summarize our experimental results on the studies of passive coherent beam combination in a specific laser cavity architecture in which a homemade binary phase Dammann grating is a key design feature. We introduce phase perturbations into the passively phase-locked array in a quasistatic manner, allowing us to make precision measurements of the cavity response to these phase errors. The self-phasing behavior is quantified and its physical origins are explained through a series of targeted measurements.

*chia0078@umn.edu; phone 1 612 625-1574

2. EXPERIMENTS

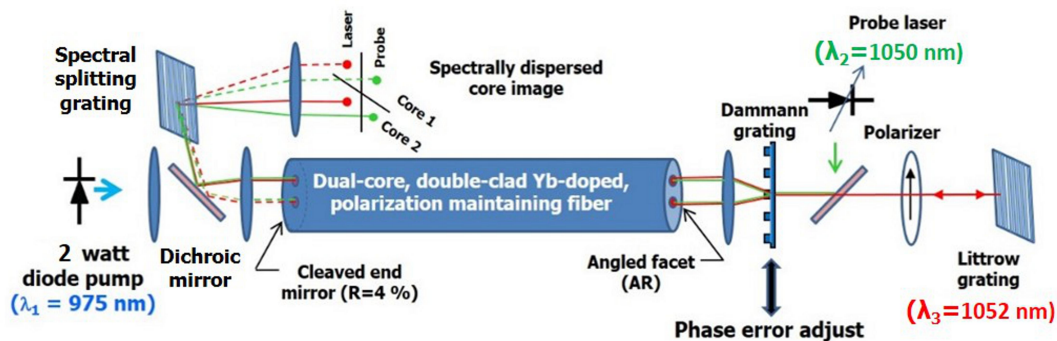


Figure 1. Laser cavity configuration and diagnostic instrumentation in our experiments.

Laser cavity architecture

Fig. 1 shows our experimental setup. The laser cavity consists of a waveguide section and a free-space section. The waveguide section is a piece of specialty fiber ~ 3 m in length custom designed and fabricated by the Optoelectronics Research Centre in Southampton. The fiber is twin-core, double-clad, and polarization-maintaining. The two identical Ytterbium-doped cores are separated by $20 \mu\text{m}$ and each has a diameter of $4 \mu\text{m}$. They are embedded in a single rectangular ($107 \mu\text{m} \times 219 \mu\text{m}$) inner-clad along with two stress rods. The two Ytterbium-doped fiber amplifiers are practically in the same thermal environment due to their proximity with each other. At the same time, they are far apart enough from one another so that evanescent coupling between them is negligible. The residual optical path length difference between the two gain arms over the entire 3 m-long fiber is further reduced to $\sim 35 \mu\text{m}$ by systematically bending and coiling the fiber. Theoretical analysis shows that differential phase adjustment between the coupled gain elements as a result of wavelength tuning is practically eliminated by the combination of this small residual optical path length difference and a limited lasing gain bandwidth (which is restricted to no more than 3 nm in our experiments by a Littrow grating). One fiber end is square-cleaved to serve as a 4% reflectivity end mirror. The other fiber end is coupled to an external cavity, *i.e.* the free-space section, and is angle-cleaved at $\sim 9^\circ$ to reduce back-reflection from this end facet.

The free-space section consists of an aspheric lens, a homemade binary phase Damann grating, a Glan-Brewster-angle polarizer, and a ruled diffraction grating. The aspheric lens collimates the light emitted from the two fiber amplifiers. The homemade binary phase Damann grating is placed at the back focal plane of this aspheric lens. It acts as a 2×1 beam combiner for light propagating in one direction (toward the right in fig. 1) and as a 1×2 beam splitter for light propagating in the opposite direction (toward to left in fig.1). The theoretical splitting (or combining) efficiency of this binary phase Damann grating is 81%. The polarizing axis of the Glan-Brewster-angle polarizer is aligned with one of the polarization-maintaining principal axes of the specialty fiber. This creates loss discrimination between the two polarization eigenmodes of the specialty fiber and therefore forces the laser cavity to oscillate only in one of the polarization eigenmodes. The ruled diffraction grating in the far end closes the laser cavity. We use the grating at its Littrow angle and therefore effectively restrict the laser gain bandwidth to less than 3 nm. The gain elements are cladding pumped at 975 nm (from the left side in fig. 1 through a dichroic mirror) by a multimode laser diode array. This laser diode array has a maximum output power of 180 W, but we only operated it at no more than 2.3 W in the experiments that we will be describing below.

Probing the laser cavity

A beam splitter (T: R=70: 30) is inserted into the free-space section midway between the binary phase Damann grating and the Glan-Brewster-angle polarizer. A probe beam generated by a tunable semiconductor laser can be injected into the laser cavity via this beam splitter. The light emerging from the square-cleaved end of the fiber is reflected off a dichroic mirror and spectrally separated by a diffraction grating. The optical signals within a chosen spectral band are then imaged onto a CCD camera. This permits observations of spectrally resolved fiber core images. By properly rearranging the imaging system, the interference fringes produced by overlapping the light from the two fiber amplifiers can be observed instead, allowing us to assess the degree of coherence and the phase difference between the two cores.

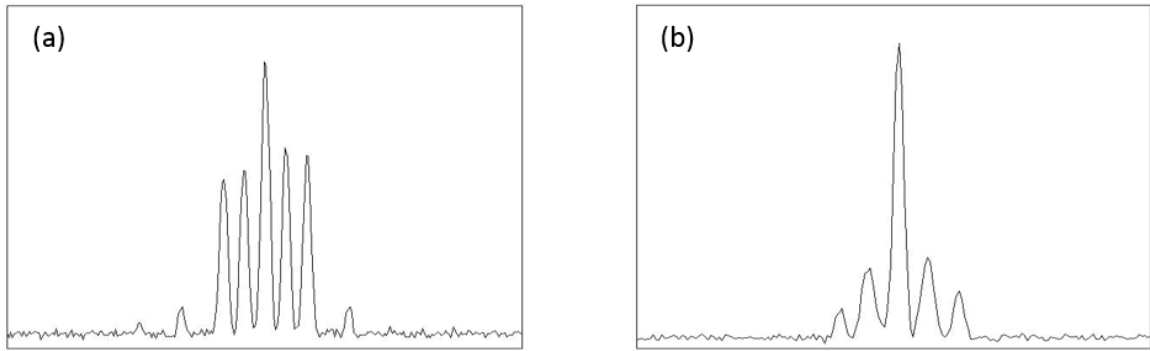


Figure 2. Far-field intensity distribution of the combined beam: (a) incoherently combined; (b) coherently combined.

Results

In addition to the differential phase internally present between the coupled fiber amplifiers, an extra amount can be added to it by a spatial translation of the binary phase Dammann grating in the direction depicted in fig. 1 (see “Phase error adjust” in figure). According to the Fourier shift theorem, a grating displacement Δx introduces a phase shift $\Delta\phi = 2\pi\Delta x/T_g$, where T_g is the grating period (~ 1.5 mm in our experiments), in the +1 diffraction order of this grating. The corresponding phase shift introduced in the -1 diffraction order is the same in magnitude but opposite in sign. Therefore, an extra 4π differential phase can be added to the coupled fiber amplifiers by a full period of grating displacement. We experimentally verified this linear relationship between $\Delta\phi$ and Δx by injecting a probe beam into the two fiber amplifiers via the binary phase Dammann grating. The data were fitted to a linear model. The regression analysis showed an adjusted R-squared of greater than 0.999.

The far-field intensity distribution of the combined beam is observed by imaging the lasing light field reflected off the beam splitter in the free-space section of the laser cavity. Fig 2 (a) shows the result of incoherent beam combining. This intensity distribution is observed, for instance, when the laser is below the lasing threshold. Fig. 2 (b) shows the result of coherent beam combining. The Littrow grating is designed to only return light from the central peak of this distribution. Proper phasing between the coupled fiber amplifiers results in dramatic concentration of energy into the on-axis wave, and a corresponding increase in the light returned to the laser cavity by the Littrow grating.

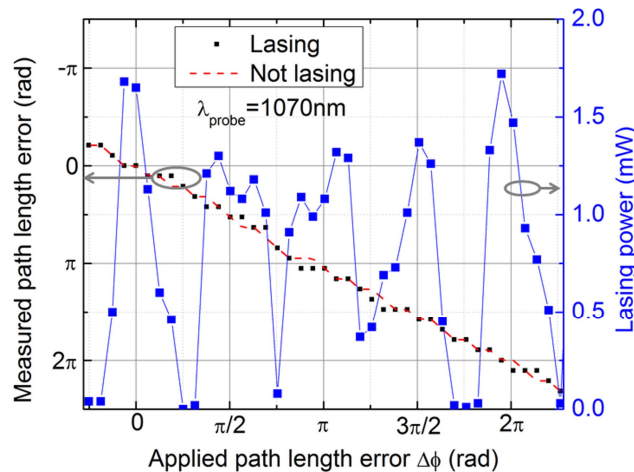


Figure 3. Total optical path length error and the lasing power at the uncombined port measured as a function of the applied path length error. The data were taken when the laser was running just above its lasing threshold.

We simultaneously measured the total (*i.e.* internal plus applied) optical path length error and the lasing power at the uncombined port (*i.e.* the optical power of the light exiting the square-cleaved fiber end) as a function of the applied path length error. Fig. 3 shows the data taken when the operating point was only slightly above the lasing threshold. The lasing wavelength of this coherently phased array was 1052 nm. The lasing power versus applied path length error data

(blue squares) has the characteristics predicted by a cold-cavity theory⁸. Lasing power varies with the applied path length error nearly periodically with a period of $\pi/2$. This is the direct consequence of a phase-error-dependent cavity loss. The total optical path length error was measured both when the laser was operating under normal conditions (black squares) and when the ruled diffraction grating was temporarily blocked (red dashed line). In both cases, the total optical path length error is always equal to the applied path length error.

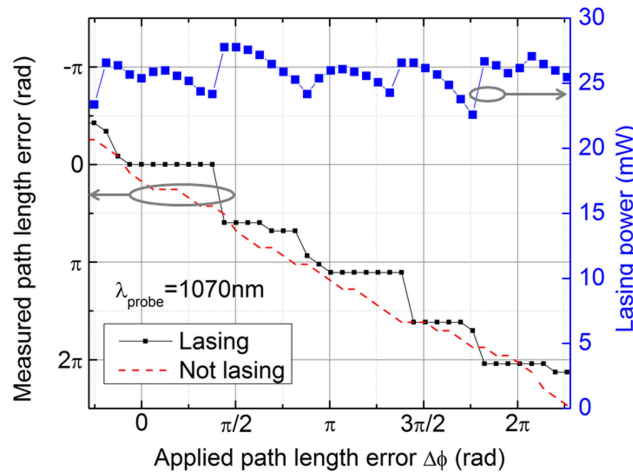


Figure 4. Total optical path length error and the lasing power at the uncombined port measured as a function of the applied path length error. The laser was running sufficiently above its lasing threshold.

We performed the same sets of measurements at a higher pump power (roughly twice the threshold pump power). Fig. 4 shows the data from these measurements. At this operating point, the lasing characteristics deviate significantly from those predicted by a cold-cavity theory. Although a $\pi/2$ -periodic modulation in the lasing power (blue squares) is still present, lasing does not stop even at the theoretically predicted applied path length errors that would result in complete cavity loss. The total optical path length error exhibits a distinct staircase-like characteristic (black squares). When the lasing was interrupted by blocking the ruled diffraction grating, the stair-case structure disappeared (red dashed line). The optical path length errors shown in fig. 3 and fig. 4 were measured at a probe wavelength of 1070 nm. We have also repeated the measurements at other probe wavelengths, such as 1050 nm and 1090 nm. The results indicate that the wavelength dependence in the measurements of the optical path length errors is practically negligible. This result is consistent with previous studies on resonant nonlinearity in Ytterbium-doped fiber⁹.

The regular phase steps shown in fig. 4 indicate that the total optical path length error is driven towards values that correspond to minimum or nearly minimum cavity loss. Since the total optical path length error is the sum of the internal optical path length error and the applied optical path length error, the stairs structure implies that there is a self-phasing mechanism in the couple fiber amplifiers which permits self-adjustment of the internal optical path length error in such a way as to maintain a phasing conditions in the minimum-loss states. In what follows, we present experimental results that led us to conclude that self-phasing under our experimental conditions is primarily due to the Kramers-Kronig effect¹⁰ (resonant nonlinearity).

First, we core-pumped one of the Ytterbium-doped fiber cores from the same side as the previous cladding pump using a single-mode laser diode at 976 nm. To prevent lasing action in the coupled fiber lasers, the ruled diffraction grating that provides optical feedback was temporarily blocked during this experiment. A probe beam at 1050 nm was injected into the fiber amplifiers via the binary phase Dammann grating. The optical power of the probe beam was chosen to be weak enough so that it did not substantially saturate the gain medium. We experimentally verified that this is so in an independent experiment. The unpumped Ytterbium-doped core served as the reference for both the phase and the gain measurements. Interference fringes as well as the core images were recorded separately by a CCD camera at various pump powers to measure the induced phase shift ϕ_{KK} as a function of the single-pass gain G . Fig. 5 presents the results of these measurements. The data shows a linear relationship between the Kramers-Kronig phase shift and the small-signal exponential gain. A Henry's alpha parameter¹¹ $\alpha = 2\phi_{KK}/\ln(G)$ value of 7.4 was extracted from a linear fit (red solid line).

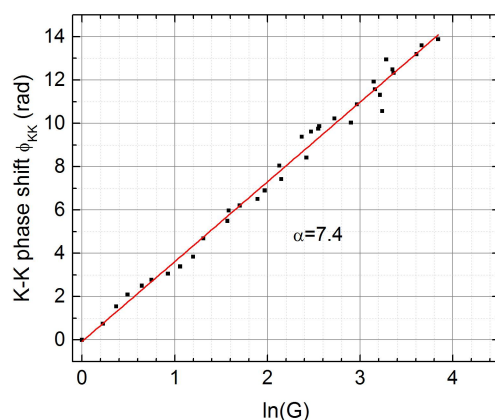


Figure 5. Kramers-Kronig phase shift versus the small-signal exponential gain $\ln(G)$. Here, G is the single-pass power gain.

Next, we characterized the gain saturation effect in each individual fiber amplifier. We cladding pumped the specialty fiber at 975 nm using the multimode laser diode array. The laser was running at a fixed pump power (roughly twice the threshold pump power) during this experiment. In order to measure the single-pass power gain, a weak probe beam at 1050 nm was also injected into the two Ytterbium-doped fiber amplifiers via the binary phase Dammann grating. The fiber core images were observed on a CCD camera. Fiber core images at different wavelengths (Ytterbium laser emission at 1052 nm and the probe signal at 1050 nm) were spatially separated but appeared in the same camera image frame. This permits simultaneous measurements of the lasing output intensity and the single-pass power gain of each individual Ytterbium-doped fiber amplifier. The spectrally resolved fiber core images were recorded at various cavity losses (and therefore various round-trip gains). Fig. 6 plots the small-signal exponential gain versus the lasing output intensity for both Ytterbium-doped fiber cores. Since the lasing output intensity is proportional to the internal energy flux density directly behind the 4% reflectivity end mirror (*i.e.* the square-cleaved fiber end facet), the data shown here is a fair assessment of the gain saturation behaviors in each individual Ytterbium-doped fiber amplifier. The solid curves are nonlinear fits to the standard gain saturation model. The differences between the two curves are very likely the results of coupling efficiency differences between the two Ytterbium-doped fiber cores at the angle-cleaved end facet.

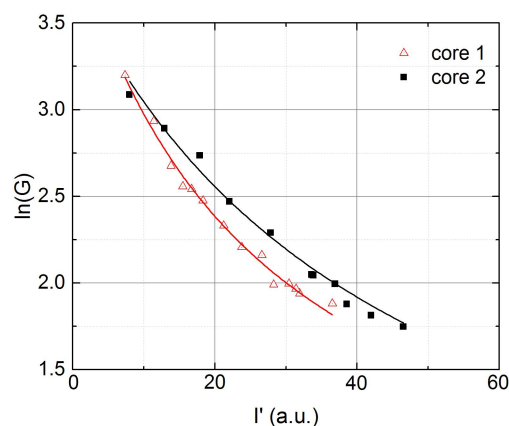


Figure 6. Small-signal exponential gain $\ln(G)$ versus the lasing output intensity I' in each individual Ytterbium-doped fiber core.

Using the same diagnostic instrumentation setup as described in the previous paragraph, we measured the lasing output intensity and the small-signal exponential gain of each individual Ytterbium-doped fiber amplifier as a function of the applied path length error. The data are presented in fig. 7.

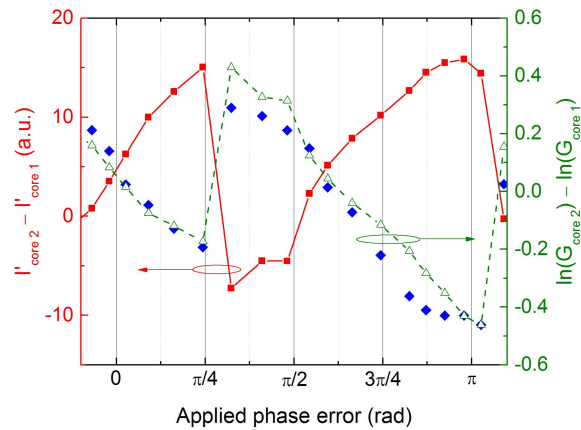


Figure 7. Difference in the lasing output intensities of the two Ytterbium-doped fiber amplifiers (red squares) and the corresponding difference in their small-signal exponential gains (blue diamonds) measured as a function of the applied path length phase error. The calculated differences in their small-signal exponential gains are presented here as green open triangles.

The difference in the lasing output intensities (red solid squares) increases discontinuously as the applied optical path length phase error increases. The discontinuous jumps occur approximately every $\pi/2$ -radian increase in the applied phase error. Here, we plot the absolute difference in the lasing output intensities rather than the relative difference because the differential Kramers-Kronig phase shift, which is what we ultimately care about, is linked to the absolute quantity. In terms of the relative difference, $(I'_2 - I'_1)/(I'_2 + I'_1)$ increases from 0 to about 33% over an applied phase error change of $\pi/2$ radians. The corresponding difference in the small-signal exponential gains (blue solid diamonds) decreases discontinuously as the applied phase error increases. The blue curve roughly mirrors the red curve, which is expected qualitatively based on the gain saturation characteristics in the two fiber amplifiers. To check this quantitatively, we calculated the difference in the small-signal exponential gains using the measured lasing output intensity data along with the gain saturation characteristics from fig. 6. The calculated results are plotted in fig. 7 as green open triangles. The quantitative agreement between the calculated results and the data from direct measurements is evident.

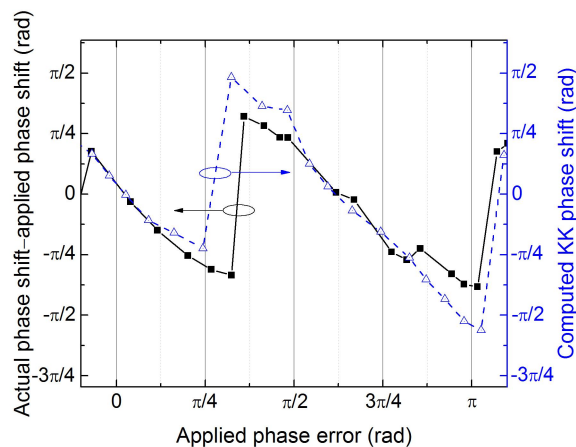


Figure 8. Experimentally observed self-phasing (black solid squares) and the computed Kramers-Kronig phase shift (blue open triangles) plotted as a function of the applied optical path length error.

The observed self-phasing can be quantified by subtracting the applied path length error (e.g. the red dashed line in fig. 4) from the total path length error (e.g. the black staircase-like structure in fig. 4). For the sake of fair quantitative comparison, we performed this subtraction on a set of data (similar to those shown in fig. 4) taken at a probe wavelength

of 1050 nm. The results are plotted in fig. 8 as black solid squares. The expected differential Kramers-Kronig phase shifts (blue open triangles) were computed and plotted in fig. 8 as well. The expected differential Kramers-Kronig phase shifts were inferred from the lasing output intensity versus the applied phase error data of both Ytterbium-doped fiber amplifiers (data the red curve in fig. 7 is based on), their gain saturation characteristics (data shown in fig. 6), and the KK-phase shift versus the small-signal exponential gain relationship (data shown in fig. 5). The correspondence between the black curve and the blue curve in fig. 8 is visible both qualitatively and quantitatively.

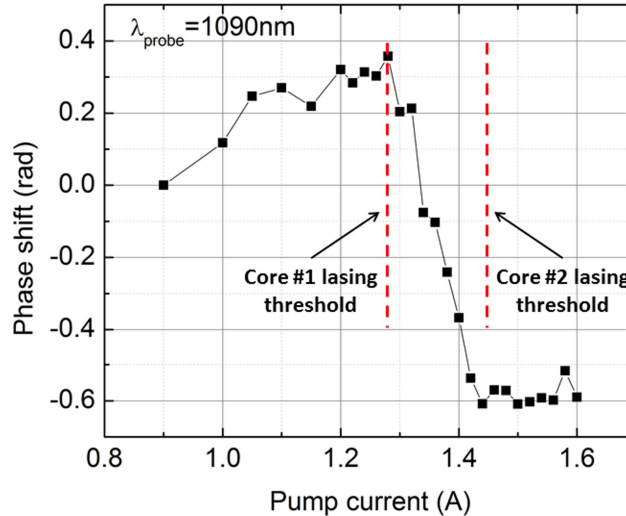


Figure 9. Measured total optical path length error versus the drive current of the 975 nm multi-mode laser diode array. The two Ytterbium-doped fiber amplifiers are allowed to lase independently and have slightly different lasing thresholds in this experiment.

Resonant (gain related) nonlinearity is not the only physical mechanism that is capable of generating a differential phase shift between the (coherently or incoherently) combined fiber amplifiers under our experimental conditions. Another set of mechanisms (including linear thermal expansion and thermal-induced change of the index of refraction) is related to the thermal load in the fiber amplifiers. In order to assess the magnitude of the thermal effects, we performed the following experiment. The same Ytterbium-doped fiber amplifiers were cladding pumped as usual. Instead of coherently coupling the two Ytterbium-doped fiber amplifiers and therefore forcing the composite laser cavity to oscillate in a supermode, we intentionally let the two gain arms lase independently and have slightly different lasing thresholds. The differential phase shift between the two gain arms was again measured by launching a probe beam into both Ytterbium-doped fiber cores. In fig. 9, we plot the measured differential phase shift as a function of the drive current of the 975 nm multimode laser diode array. The pump power was roughly 2.3 W when the drive current reached 1.6 A.

The data can be divided into three regions from left to right. In the first region, both gain arms are below their respective lasing thresholds. The moderate positive slope is most likely due to slightly different pumping or loss conditions in the two Ytterbium-doped fiber cores. In the second region, one of the gain arms is lasing and the other gain arm is still below the threshold. The gain related phase shift in the lasing arm is clamped due to gain clamping at threshold. The steep negative slope is the result of gain related phase shift still changing in the below-threshold gain arm. In the third region, both gain arms are lasing and therefore there will be no further changes of gain related phase shifts in both Ytterbium-doped fiber cores. The differential phase shift in this third region can be purely attributed to thermal effects. We fit the data in region 3 to a linear model and obtained the rate of differential phase change of roughly 0.16 radians per ampere of drive current (or approximately 0.086 radians per watt of pump power). This leads to a plausible estimate of the upper bound of thermal-biased differential phase shift of about 0.198 radians (or roughly $\pi/16$ radians) at 2.3 W of pump power. All the experiments described in this paper were performed at pump power levels less than 2.3 W.

3. CONCLUSIONS

In this paper, we summarize our experimental results on passive coherent beam combining in a specific laser cavity architecture. We observed self-phasing in coherently coupled Ytterbium-doped fiber amplifiers above a certain pump power level. We traced the origin of this self-phasing to the resonant (gain related) nonlinearity in the fiber amplifiers.

The results presented here are unique in the sense that self-phasing in passively coherently coupled fiber amplifiers are explicitly linked to the differential Kramers-Kronig phase shift in a quantitative manner. To the best of our knowledge, this aspect had never been demonstrated experimentally before.

Experimentally, we observed that the intensity distribution in the supermode (in other words, the lasing output intensity distribution between the coherently coupled fiber amplifiers) changes as the applied path length error changes. This is a feature that is not predicted by a simple passive-cavity theory. A theoretical model, taking into account Kerr and resonant nonlinearities, was recently proposed by Bochove, Zunoubi, and Corcoran¹². It is possible that more realistic computer simulations can be carried out based on their theoretical framework.

REFERENCES

- [1] Yu, C. X., Augst, S. J., Redmond, S. M., Goldizen, K. C., Murphy, D. V., Sanchez, A. and Fan, T. Y., "Coherent combining of a 4 kW, eight-element fiber amplifier array," *Opt. Lett.* 36(14), 2686-2688 (2011).
- [2] Jeux, F., Desfarges-Berthelebot, A., Kermene, V. and Barthelemy, A., "Efficient passive phasing of an array of 20 ring fiber lasers," *Laser Phys. Lett.* 11, 095003 (4pp) (2014).
- [3] Corcoran, C. J., Durville, F. and Pasch, K. A., "Coherent array of nonlinear regenerative fiber amplifiers," *IEEE J. Quantum Electron.* 44(3), 275-282 (2008).
- [4] Corcoran, C. J. and Durville, F., "Passive phasing in a coherent laser array," *IEEE J. Sel. Top. Quantum Electron.* 15(2), 294-300 (2009).
- [5] Napartovich, A. P., Elkin, N. N. and Vysotsky, D. V., "Influence of non-linear index on coherent passive beam combining of fiber lasers," *Proc. SPIE* 7914, 791428 (10pp) (2011).
- [6] Corcoran, C. and Durville, F., "Passive coherent combination of a diode laser array with 35 elements," *Opt. Express* 22(7), 8420-8425 (2014).
- [7] Guillot, J., Desfarges-Berthelebot, A., Kermene, V. and Barthelemy, A., "Experimental study of cophasing dynamics in passive coherent combining of fiber lasers," *Opt. Lett.* 36(15), 2907-2909 (2011).
- [8] Chiang, H.-S., Leger, J. R., Nilsson, J. and Sahu, J., "Direct observation of Kramers-Kronig self-phasing in coherently combined fiber lasers," *Opt. Lett.* 38(20), 4104-4107 (2013).
- [9] Arkwright, J. W., Elango, P., Atkins, G. R., Whitbread, T. and Dignonnet, M. J. F., "Experimental and theoretical analysis of the resonant nonlinearity in Ytterbium-doped fiber," *J. Lightwave Technol.* 16(5), 798-806 (1998).
- [10] Chiang, H.-S., Nilsson, J., Sahu, J. and Leger, J. R., "Experimental measurements of the origin of self-phasing in passively coupled fiber lasers," *Opt. Lett.* 40(6), March 15 (2015).
- [11] Henry, C. H., "Theory of the linewidth of semiconductor lasers," *IEEE J. Quantum Electron.* QE-18(2), 259-264 (1982).
- [12] Bochove, E. J., Zunoubi, M. R. and Corcoran, C. J., "Effect of Kerr and resonant nonlinearities on phase locking of multistable fiber amplifier array," *Opt. Lett.* 38(23), 5016-5019 (2013).